Journal of Chromatography A 1775 (2026) 466913

Contents lists available at ScienceDirect

Journal of Chromatography A

journal homepage: www.elsevier.com/locate/chroma

Beyond compound-specific methods: Group-specific UHPLC-MS/MS enables rapid detection and quantitation of all glucosinolates

Ville Fock *, Niko Luntamo, Juha-Pekka Salminen

Natural Chemistry Research Group, Department of Chemistry, University of Turku, FI-20014 Turku, Finland

ARTICLE INFO

Keywords:
Glucosinolate
Mass spectrometry
LC-MS/MS
MRM
PRM
Group-specific

ABSTRACT

Glucosinolates are widely consumed specialized metabolites predominantly found in the Brassicaceae family. Existing analytical methods typically target only specific subsets of glucosinolates and therefore lack the versatility required for comprehensive glucosinolate screening. Hence, there is a gap in analytical methods targeting glucosinolates that can detect any glucosinolate within a given matrix. In this study, targeted compound group-specific multiple reaction monitoring (MRM) and parallel reaction monitoring (PRM) methods were developed and validated for comprehensive qualitative and quantitative profiling of glucosinolates. Among all glucosinolate group-specific fragment ions evaluated, five (*m/z* 96, 97, 241, 259, and 275) were selected for product ion optimization and method validation. Of the fifteen transitions selected for method validation, four were retained in the final MRM method based on sensitivity and selectivity. Additionally, the performances of the group-specific methods were compared against simultaneously created compound-specific MRM methods. Although the more traditional compound-specific methods offered slightly improved sensitivity, they were limited to detect only individual glucosinolates. While detecting whole glucosinolate groups, the group-specific MRM methods showed lowest limits of detection (LOD) ranging from 11.5 to 87.3 ng/mL, and the upper limits of quantitation (ULOQ) from 2.5 to 55 μg/mL. High-resolution group-specific PRM methods enabled accurate glucosinolate characterization and yielded LODs for the best precursor ion *m/z* 259 between 44.1 and 473.6 ng/mL, with ULOQs ranging from 8 to 50 μg/mL. Application of the methods demonstrated their capability to detect 51 distinct glucosinolates across 19 plant species.

1. Introduction

Glucosinolates are a well-documented group of specialized metabolites produced predominantly by plants in the order *Brassicales*, especially within the Brassicaceae family, including important crops such as cabbage (*Brassica oleracea*), rapeseed (*Brassica napus*), and mustard (*Sinapis alba*). They play essential roles in food chemistry and in plant defense through their hydrolysis products. In addition, glucosinolates and their degradation products have been associated with potential health-promoting properties, including anticancer, antimicrobial, and anti-inflammatory effects [1]. However, their abundance varies significantly between species and even among plant tissues. On average, they constitute approximately 1% of plant dry weight [2], although exceptionally high levels, up to 25% of dry weight, have been reported in moringa tree (*Moringa oleifera*) [3]. To address this variability and enhance the potential health benefits of glucosinolates, breeding strategies have been developed to increase the glucosinolate content in cultivars [4].

Structurally, glucosinolates share a common core structure consisting of a *β*-D-thioglucose moiety and a sulfonated oxime group, while their structural diversity arises from variable side chains. They can be classified into three major subgroups based on their amino acid precursors and structural features: aliphatic, aromatic, and indole glucosinolates (Fig. 1). These subclasses originate from at least ten different amino acids. Specifically, indole glucosinolates are mainly derived from tryptophan, aromatic glucosinolates predominantly from phenylalanine or tyrosine, and aliphatic glucosinolates primarily from methionine, valine, leucine, or isoleucine [5,6]. The diversity of precursor amino acids and side group modifications contribute to the wide structural variability observed within this compound family. To date, over 130 naturally occurring glucosinolates have been identified in plants [5,7,8].

Traditionally, glucosinolates have been analyzed by UV detection at wavelengths between 225 and 235 nm [9–12], although this approach is hindered by limited sensitivity and selectivity. The application of mass

* Corresponding author.
E-mail address: ville.a.fock@utu.fi (V. Fock).

https://doi.org/10.1016/j.chroma.2026.466913
Received 11 February 2026; Received in revised form 18 March 2026; Accepted 19 March 2026
Available online 20 March 2026

spectrometry has significantly advanced glucosinolate analysis, with tandem mass spectrometry (MS/MS) becoming the standard for both qualitative and quantitative applications [13–20]. Their analyses can be conducted in either positive or negative ion mode, depending on whether glucosinolates are measured in their intact form or after desulfonation [14,21]. Although positive ionization has been applied successfully, the desulfonation process has been shown to be laborious and time-consuming [10,13,15,22–25]. Due to the complexity of the desulfonation process and the anionic nature of the sulfonate group (Fig. 2), negative ionization has become the preferred mode for glucosinolate detection [3,11,13–17,26–42]. In addition, several diagnostic fragments, including sulfuric acid and glucose 1-thiosulfate anions (Fig. 2), are exclusively observed in negative ion mode [14,15].

Negative ionization plays a central role in glucosinolate analysis, as shown by its widespread use in the literature, where hydrogen sulfate ion (*m/z* 97), along with its related fragments (Fig. 2A) are the most commonly employed product ions in MS analysis [14,17,26,30,31,37,38,40,42,43]. However, despite their high abundance, these ions lack specificity to glucosinolates as they can also originate from other sulfate-containing compounds via cyclic syn-elimination [44]. Therefore to improve selectivity, glucosinolate-specific fragments such as *m/z* 259 and 195 (Fig. 2B) have been utilized as product ions in compound-specific multiple reaction monitoring (MRM) assays [29,45]. Furthermore, glucosinolates have been shown to produce characteristic compound-specific fragments, including consistent neutral losses such as $[M-242-H]^-$ (Fig. 2C) and $[M-196-H]^-$ or $[M-193-H]^-$ [7,14,18]. These unique fragmentation patterns form the foundation for targeted detection strategies commonly implemented through MRM approaches.

MRM methods have become widely used in quantitative analyses due to their high sensitivity and reproducibility. Yet, existing MRM methods for glucosinolates rely on compound-specific approaches, limiting detection only to a subset of compounds [10,13,16,29–31,36,38,42,45]. To overcome this limitation of compound-specific methods, group-specific strategies have been employed to other specialized metabolites [46–49]. These approaches utilize characteristic fragment ions shared within structural classes or specific subsets enabling broader detection without compound-specific optimization. However, the low-resolution MRM limits its scope, prompting interest in high-resolution alternatives such as parallel reaction monitoring (PRM).

High-resolution MS/MS methodologies have introduced PRM as a powerful alternative to traditional MRM methods [50]. While PRM is widely used in proteomics, its application in plant metabolomics has gradually increased over the past decade [18,39,51–53]. Unlike MRM, PRM generates an MS/MS spectrum of all fragment ions for each precursor ion, requiring careful validation of compound identification. However, by utilizing ubiquitous glucosinolate fragments such as *m/z* 74.99, 96.96, and 259.01, accurate detection by PRM is possible [18]. Although PRM offers enhanced accuracy and structural confirmation, it has not yet been systematically applied to glucosinolate profiling, particularly with group-specific detection strategies.

In this study, we present novel group-specific UHPLC-MS/MS methods for the detection and quantitation of glucosinolates. The methods were developed for triple quadrupole MS (TQ-MS) and hybrid Q-Orbitrap-MS instruments, utilizing MRM and PRM methodologies, respectively. We describe the advantages and limitations of both approaches: the high-speed but lower-resolution TQ-MS and the slower yet highly accurate Orbitrap system. Method validation was performed to ensure analytical robustness and the applicability of the methods was demonstrated using extracts of 19 plant species. These methods aim to overcome limitations of the compound-specific methods by employing ubiquitous glucosinolate fragments as precursor ions, enabling broader detection across the entire compound group. This strategy provides a rapid, sensitive, and robust framework for glucosinolate analysis while supporting the identification of previously uncharacterized compounds.

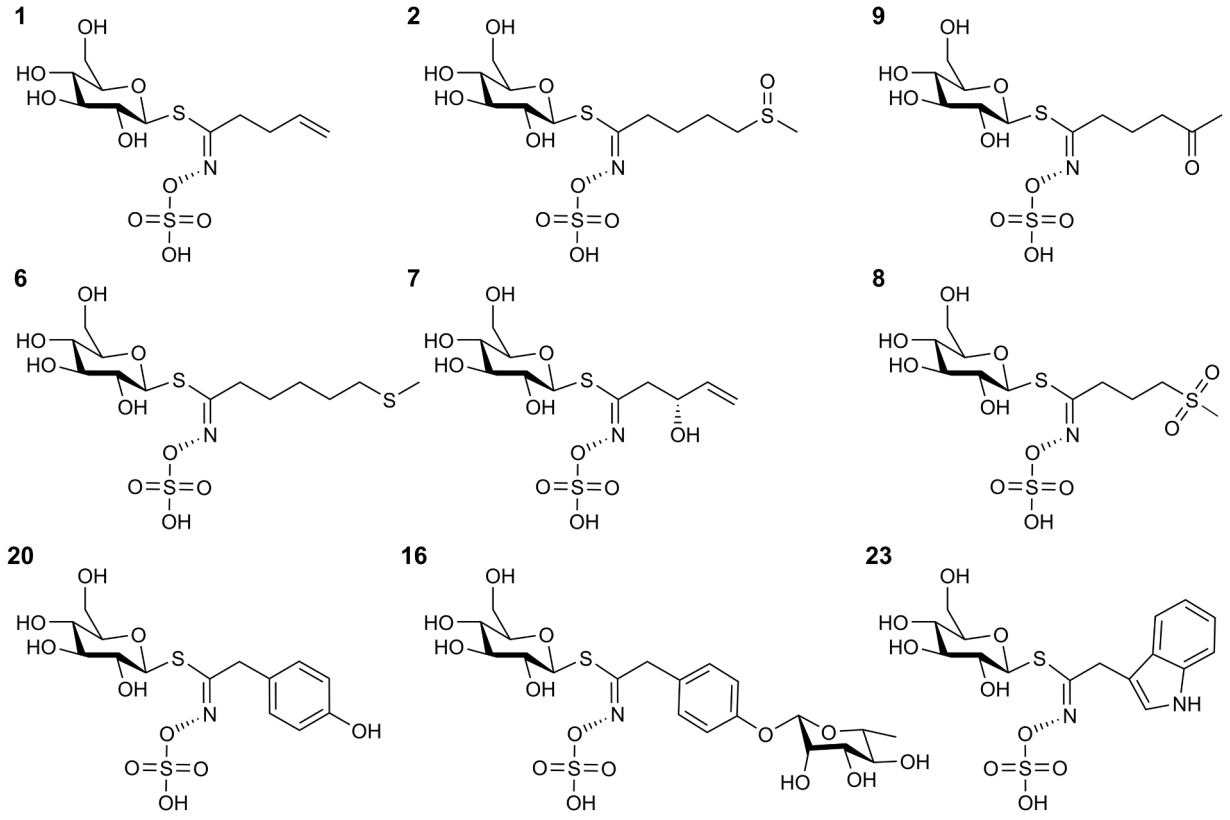

Fig. 1. Example structures of glucosinolates, where 1, 2, and 6–9 are aliphatic glucosinolates, 16 and 20 are aromatic glucosinolates, and 23 is an indole glucosinolate. Corresponding compound numbers are listed in Table 1.

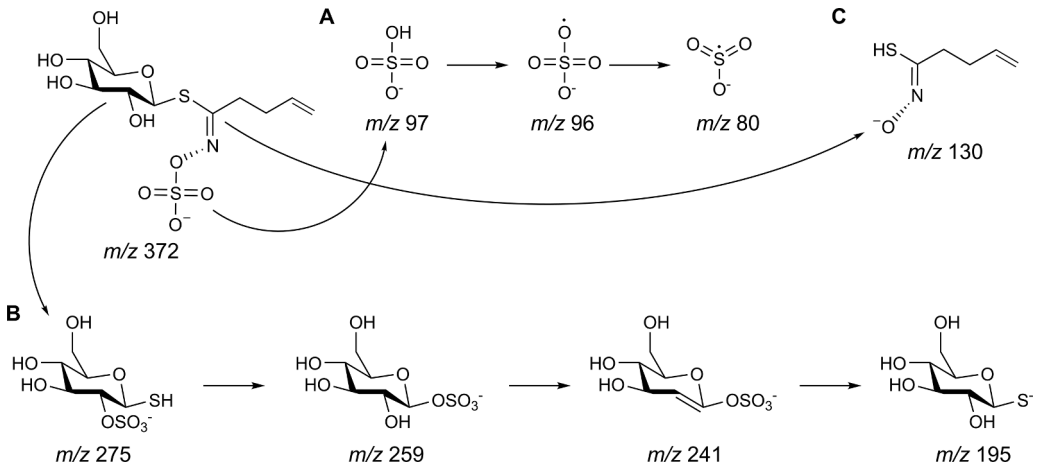

Fig. 2. Glucosinolate fragmentation illustrated with gluconapin, where A shows the fragmentation of hydrogen sulfate and its fragments, B shows thioglucose and sulfate structure along with their fragments, and C shows the compound-specific fragment M−thioglucose−sulfur trioxide ([M−242−H]$^-$).

2. Materials and methods

2.1. Chemicals and reagents

Acetonitrile (Fisher Chemical, Waltham, MA, USA), LC-MS grade formic acid (VWR, Radnor, PA, USA), and ultrapure water (Merck Millipore Synergy UV instrument) were used in the UHPLC-MS analyses. 3 mM aqueous HCl used for sample dissolution was prepared from analytical grade hydrochloric acid (34%, V/V) obtained from VWR (Radnor, PA, USA). All standards were purchased from Extrasynthese (Genay, Bourgogne, France) (Fig. 3 and Table 1).

2.2. Plant materials

Plant materials were collected from the Botanical Garden of the University of Turku (Ruissalo, Turku, Finland). The plant materials collected were leaves of *Brassica juncea* 'Bloody Mary', *B. juncea* 'Crimson Red', *B. juncea, B. juncea* 'Moutarde Rouge Métis', *Brassica rapa, B. rapa* 'Tatsoi Red', *B. rapa* subsp. *nipposinica, Brassica napus, Brassica nigra, Camelina sativa, Sinapis alba, Eruca sativa, Eruca vesicaria, Rhamphospermum arvense, Arabis caucasica, Iberis pruitii, Crambe maritima, Draba hispanica, Raphanus sativus* var. *niger*, and *Lepidium sativum*. The plant materials were frozen after collection and freeze-dried with Christ Beta 2–8 LD plus (Martin Christ Gefriertrocknungsanlagen GmbH, Osterode am Harz, Germany) overnight or until completely dry. The dried material was ground into a fine homogeneous powder using a ball-mill.

Matrix effects were evaluated using a plant extract mixture containing leaves of *Vaccinium vitis-idaea, Geranium sylvaticum, Rubus chamaemorus, Betula pubescens, Quercus robur, Rubus idaeus*, and *Pinus sylvestris*, as well as flowers of *Lysimachia vulgaris* and *Trifolium medium*. Additionally, the methods were tested for selectivity and specificity measurements with a plant extract mixture containing leaf extracts of *Filipendula ulmaria, Punica granatum, Geum urbanum, Terminalia chebula, Rosa spinosissima* 'Plena', *Lythrum salicaria, Rosa rugosa*, and *Salix phylicifolia*, together with needle extract of *Pinus sylvestris*.

2.3. Sample extraction and preparation

Freeze-dried and ground plant samples (20 mg) were weighed into 2 mL Eppendorf tubes. 1400 µL acetone/water (80/20, V/V) was added to each tube, followed by vortexing briefly prior to overnight maceration at 4 °C. After maceration, tubes were shaken for 3 h using a planar shaker, centrifuged, and supernatants were transferred to new 2 mL Eppendorf tubes. Supernatants were evaporated to remove acetone. Remaining extraction residue was re-extracted with an additional 1400 µL of acetone/water (80/20, V/V) as above and sample-specific supernatants were pooled. Pooled extracts were concentrated until all acetone was evaporated. Extracts were frozen and freeze-dried overnight. Dried residues were reconstituted in 1000 µL of 3 mM aq. HCl solution. Prior to UHPLC-DAD-MS analysis, samples were filtered through 0.20 µm polytetrafluoroethylene (PTFE) syringe filters.

Standards (1 mg) were weighed and dissolved in 3 mM aq. HCl solution. Effect of solvent on analyte responses was evaluated using UHPLC-DAD-TQ-MS, confirming that 3 mM aq. HCl solution did not influence analyte signals compared to ultrapure water.

2.4. UHPLC-DAD-ESI-TQ-MS

MRM methods were developed using a Waters Xevo® triple quadrupole (TQ) mass spectrometer (Waters Corp., Milford, MA, USA) coupled to a Waters Acquity ultra-performance liquid chromatography (UPLC™) system (Waters Corp., Milford, MA, USA). The UPLC™ system consisted of a binary pump, column oven, diode array detector (DAD), and an autosampler equipped with a 5 µl loop injector. Chromatographic separation was performed using an Acquity UPLC® BEH C6-Phenyl column (2.1 × 100 mm, 1.7 µm particle size; Waters Corp., Wexford, Ireland). The flow rate was set to 0.500 mL/min. The gradient elution was performed using two mobile phases: acetonitrile (A) and 0.1% aqueous formic acid (B). The gradient was as follows: 0–0.5 min, 0.1% A; 0.5–5.0 min, linear increase from 0.1% to 30% A; 5.0–6.0 min, linear increase from 30% to 35% A; 6.0–9.5 min, column washing and re-equilibration. Ultraviolet-Visible (UV–Vis) data were acquired in wavelength range of 190–500 nm. In addition to the gradient methods, 2- and 3-min isocratic methods were used, employing 30% acetonitrile (A) as the mobile phase, for CV and CE optimizations. Analyses were performed either from 700 µL round-bottom 96-well plates or from 200 µl glass inserts. The injection volume was 5 µL. In negative electrospray ionization mode (ESI−), the full scan mass-to-charge (m/z) range was set to 50–1200 Da. The ionization was achieved with a capillary voltage of 1.80 kV and a cone voltage of 30 V. The desolvation gas flow rate was set to 1000 l/h and the cone gas flow to 100 l/h, both using nitrogen. The ion source temperature was set to 150 °C, the desolvation gas temperature to 650 °C, and the ion guide voltage to 3.00 V. Argon was used as the collision gas. The column oven temperature was maintained at 40 °C and the sample manager at 20 °C.

2.5. UHPLC-DAD-HESI-Q-Orbitrap-MS

PRM methods were developed utilizing a high-resolution hybrid quadrupole-Orbitrap tandem mass spectrometer (Q Exactive™, Thermo

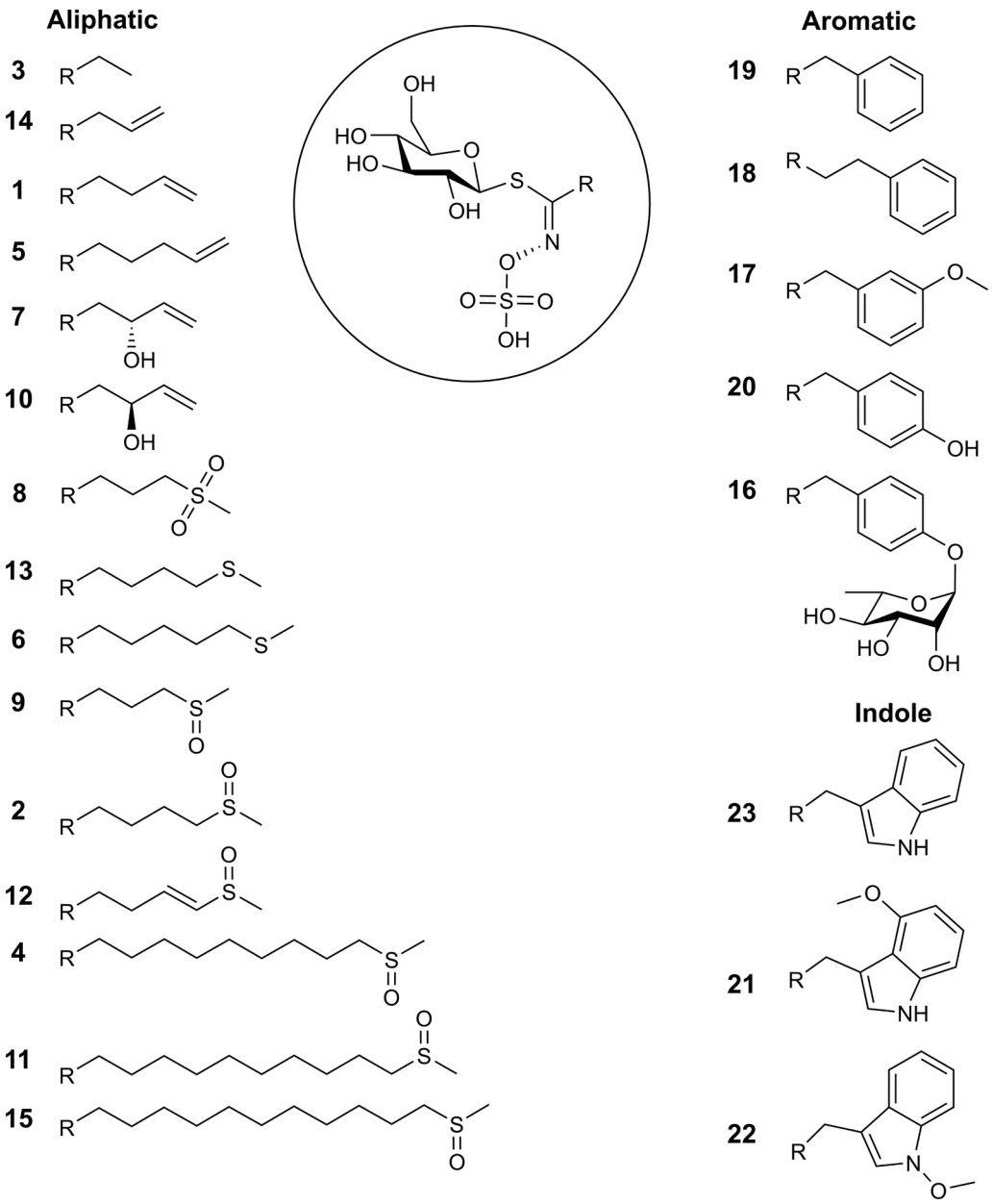

Fig. 3. Compounds utilized in the study. Corresponding compound numbers are listed in Table 1.

Fisher Scientific GmbH, Bremen, Germany) coupled to a UPLC™ system (Waters Corp., Milford, MA, USA). The UPLC™ system consisted of a binary pump, column oven, diode array detector (DAD), and an auto-sampler equipped with a 5 µl loop injector. Two lengths of analytical columns were used: Acquity UPLC® BEH C6-phenyl column (Waters Corp., Wexford, Ireland) with dimensions of 2.1 × 30 mm and 2.1 × 100 mm, both with a particle size of 1.7 µm. A flow rate of 0.500 mL/min was used for the 100 mm column and 0.650 mL/min for the 30 mm column. The gradient for 100 mm column is described in Section 2.4. and the gradient for 30 mm column was as follows: 0–0.1 min, 1% A; 0.1–3.8 min, linear increase from 1% to 33% A; 3.8–5.0 min, column washing and re-equilibration. UV–Vis data were acquired in wavelength range of 190–500 nm. Sample injections (5 µL) were performed from either 700 µL round-bottom 96-well plates or from 200 µl glass inserts. Mass spectrometric data were acquired using negative ion mode with heated electrospray ionization (HESI−). Full scan/dd-MS^2 (TopN) method was employed, where the full scan data were collected over a m/z range of 50–750 Da with a resolution of 70,000. In addition to full scan acquisition, a data dependent MS^2 (dd-MS^2) method was employed for the three most intense ions, which were selected for fragmentation at three different normalized collision energies (NCE) (30, 50, and 80 eV). The resolution for TopN data acquisition was set to 17,500. The group-specific PRM method was also performed at a resolution of 17,500. In the HESI source, the capillary temperature was set to 380 °C. The sheath gas flow rate was set to 60 units and the auxiliary gas flow rate to 20 units. Both gases were nitrogen. The spray voltage was 3.80 kV and the auxiliary gas heater temperature was 300 °C. The column oven was maintained at 40 °C and the sample manager at 20 °C.

2.6. Method development and validation

MRM methods cone voltages (CV) and collision energies (CE) were optimized using 100 µg/mL standard solutions. Optimization was based on peak height or peak area using MassLynx software (version V4.2 SCN982, Waters). CVs were evaluated at six voltages from 20 to 120 V in 20 V increments and CEs across nine energy levels, ranging from 10 to

Table 1
Compounds used in the study and their corresponding numbers, subgroups, side groups, trivial names, and molecular masses (Da).

Number	Subgroup	Side group	Trivial name	Molecular mass (Da)
1	Aliphatic	but-3-enyl	Gluconapin	373.4
2	Aliphatic	(R_s)-4-(methylsulfinyl)butyl	Glucoraphanin	437.5
3	Aliphatic	ethyl	Glucolepidiin	347.4
4	Aliphatic	(R_s)-9-(methylsulfinyl)nonyl	Glucoarabin	507.6
5	Aliphatic	pent-4-enyl	Glucobrassicanapin	387.4
6	Aliphatic	5-(methylthio)pentyl	Glucoberteroin	435.5
7	Aliphatic	(*S*)-2-hydroxy-but-3-enyl	Epiprogoitrin	389.4
8	Aliphatic	3-(methylsulfonyl)propyl	Glucocheirolin	439.5
9	Aliphatic	(R_s)-3-(methylsulfinyl)propyl	Glucoiberin	423.5
10	Aliphatic	(*R*)-2-hydroxy-but-3-enyl	Progoitrin	389.4
11	Aliphatic	(R_s)-10-(methylsulfinyl)decyl	Glucocamelinin	521.7
12	Aliphatic	(R_s)-4-(methylsulfinyl)but-3-enyl	Glucoraphenin	435.5
13	Aliphatic	4-(methylthio)butyl	Glucoerucin	421.5
14	Aliphatic	prop-2-enyl/allyl	Sinigrin	359.4
15	Aliphatic	(R_s)-11-(methylsulfinyl)undecyl	Homoglucocamelinin	535.7
16	Aromatic	4-(α-L-rhamnopyranosyloxy)benzyl	Glucomoringin	571.6
17	Aromatic	3-methoxybenzyl	Glucolimnanthin	439.5
18	Aromatic	phenethyl/2-phenylethyl	Gluconasturtiin	423.5
19	Aromatic	benzyl	Glucotropaeolin	409.4
20	Aromatic	4-hydroxybenzyl	Sinalbin	425.4
21	Indole	4-methoxyindol-3-ylmethyl	4-Methoxyglucobrassicin	478.5
22	Indole	1-methoxyindol-3-ylmethyl	Neoglucobrassicin	478.5
23	Indole	indol-3-ylmethyl	Glucobrassicin	448.5

50 eV in 5 eV increments. Additionally, further CE testing was performed using MRM methods with collision energies ranging ±10 eV around the optimized value, in 5 eV increments within 10–40 eV range. For the PRM methods, collision-induced dissociations (CID) and normalized collision energies (NCEs) were optimized using 16–20 µg/mL standard solutions. CIDs were evaluated at six energy levels (0–100 eV, 20 eV increments) and NCEs between 20 and 120 eV (20 eV increments). Optimizations were carried out in Xcalibur Qual Browser software (version 4.1.31.9, Thermo Fisher Scientific) based on peak height intensity.

The MRM and PRM methods were validated using 11 calibration points between 193 pg/mL and 100 µg/mL. Validation included limits of detection (LOD), limits of quantification (LOQ), and upper limits of quantitation (ULOQ). LOD and LOQ were calculated using equations 3.3 $\times \sigma/S$ and 10 $\times \sigma/S$, respectively, where σ represents the standard error of y-intercept and S the slope of the calibration curve [54]. These values were calculated from the linear range using the LINEST function in Microsoft Excel (version 1808). The ULOQ was determined by visual inspection and evaluation of heteroscedasticity [54–56]. Repeatability was evaluated with ten replicate injections: 1 µg/mL for the TQ-MS and 2 µg/mL for the HR-MS. Precision was expressed as relative standard deviation (RSD). In dilution series and repeatability tests, standard compounds 2, 4, 5, 11, 15, and 23 (Table 1) at 20 µg/mL were used as quality control samples. Matrix effect were calculated using equation ME (%) = $B/A \times 100$, where A represent the peak area of analyte in pure solution sample and B the peak area of analyte in matrix-spiked sample [57]. Matrix effects were evaluated in high-concentration range, i.e., the four highest measurement points (~8–100 µg/mL), and in medium-concentration range, the fifth highest measurement point (~ 3 µg/mL). Matrix effect and repeatability measurements were used to evaluate the reliability of the quantitative performance. Accuracy and robustness assessments were not included.

3. Results and discussion

3.1. Characterization of glucosinolates

Glucosinolate analysis started by finding the most suitable ionization mode. Based on UHPLC-MS measurements, negative ionization provided higher signal intensity and produced distinctively characteristic fragment ions compared to positive ionization. This observation aligns with previous reports where intact glucosinolates have been analyzed predominantly in negative ion mode [3,11,13–18,22,26–31,40–42]. In ESI−, the mass spectra displayed the deprotonated molecule $[M-H]^-$ without adduct formation and showed abundant group-specific fragments at m/z 275, 259, 241, 97, 96, 80, and 75 (Fig. 1) [14,29]. Conversely, positive ionization did not yield the protonated molecule ion $[M+H]^+$ or any related adducts for all compounds. Although $[M+H]^+$ was often absent, the adduct $[M-242+H]^+$, i.e., loss of sulfur trioxide and thioglucose, was consistently observed at a CV of 20 V [11].

Moreover, utilizing negative ionization enabled the accurate characterization of glucosinolates, even for isobaric compounds (Fig. 4). For example, 4-methoxyglucobrassicin and neoglucobrassicin were distinguished not only by retention time but also by the fragment ion m/z 446 $[M-CH_3O-H]^-$ which is absent in the 4-methoxyglucobrassicin spectrum (Fig. 4A) [11,17,29]. Similarly, although pairs such as gluconasturtiin/glucoiberin (mass difference 78 ppm), glucoberteroin/glucoraphenin (84 ppm), and glucolimnanthin/glucocheirolin (75 ppm) differ in exact mass, they also produce distinct fragments, allowing differentiation even with low-resolution MS (Fig. 4). Notably, glucolimnanthin and glucocheirolin exhibited differences only in ion ratios and in the low abundance m/z 420 fragment ion (Fig. 4D). The only isobaric compound pair that could be distinguished solely by retention time and not by MS were epiprogoitrin and progoitrin (*S*- and *R*-isomers, respectively).

On the other hand, UV-spectroscopic detection has also been applied for the detection of glucosinolates [9–12]. However, due to weak chromophores [58], their UV signals are often overlapped by other compounds in the matrix, limiting their applicability in many matrices. Interestingly, UV spectral data obtained from pure standard solutions revealed distinguishable patterns among glucosinolate subclasses, allowing for their differentiation (Fig. S1). Aliphatic glucosinolates typically exhibit a maximum absorbance in the range of 225–230 nm, occasionally accompanied by an additional band near the wavelength range 190–195 nm. Aromatic glucosinolates typically exhibit a maximum around 190–200 nm, and depending on the substituent, additional absorption bands may appear between 220 and 230 nm and 270–280 nm, as observed in compounds such as glucomoringin, glucolimnanthin, and sinalbin, which contain either a hydroxyl group or an ether linkage in the benzene ring. In contrast, aromatic glucosinolates with only a benzyl side group, such as gluconasturtiin and glucotropaeolin, display a maximum near 195 nm, followed by a gradual decrease in absorbance toward wavelength 250 nm. Indole glucosinolates, on the other hand, exhibit a maximum around 220–225 nm and a

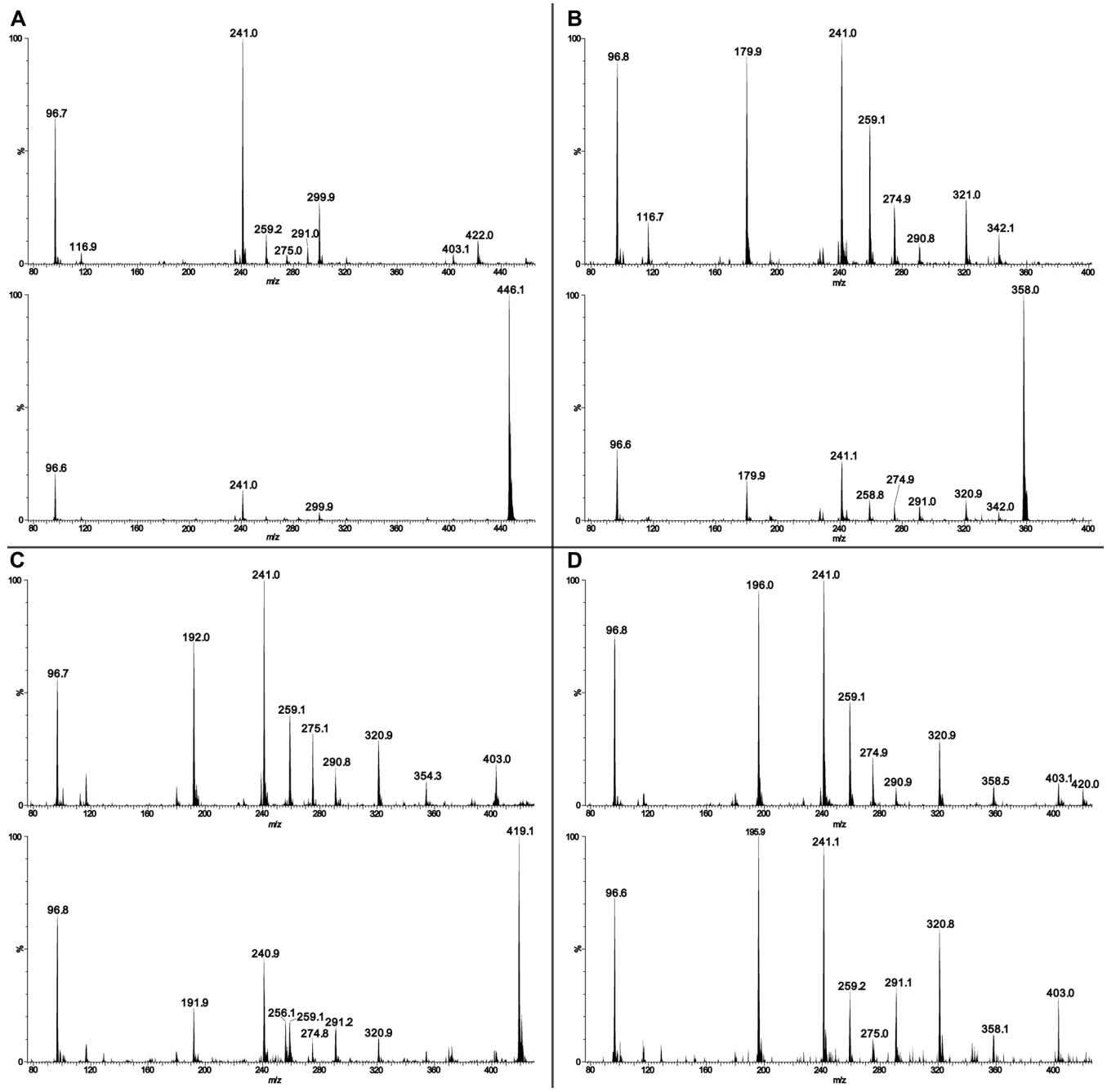

Fig. 4. Differences between 4-methoxyglucobrassicin (upper) and neoglucobrassicin (lower) (A), gluconasturtiin (upper) and glucoiberin (lower) (B), glucoberteroin (upper) and glucoraphenin (lower) (C), and glucolimnanthin (upper) and glucocheirolin (lower) (D) in TQ-MS full scan spectra.

secondary, less intense absorption band within the 260–300 nm region.

Most of the glucosinolates could also be differentiated based on retention times. The retention times ranged from 0.85 to 5.04 min (Table 2) under the gradient described in Section 2.4. Aliphatic glucosinolates showed the shortest and longest retention times, reflecting increased hydrophobicity with longer side chains. Indole glucosinolates eluted between 3.23 and 4.45 min, with glucobrassicin exhibiting the shortest retention time due to its ether linkage. Aromatic glucosinolates eluted between 1.82 and 3.65 min, with sinalbin (hydroxyl group) showing the shortest retention time and gluconasturtiin (phenethyl side chain) the longest (Fig. 3, Table 2).

3.2. MRM method development

Multiple reaction monitoring (MRM) methods were developed on Waters Xevo triple quadrupole mass spectrometer for both group-specific and compound-specific analyses. The compound-specific methods were developed to evaluate the performance of the group-specific methods in comparison with the conventional compound-specific approaches. For the group-specific approach, fragment ions *m/z* 275, 259, 241, 97, and 96 (Fig. 1), as well as *m/z* 80 and 75, were initially selected as precursor ions. For compound-specific methods, the most abundant ion, which in all cases was the deprotonated molecular ion, was chosen as the precursor (Table S1).

Group-specific cone voltage (CV) optimization revealed only minor differences among the compounds (Fig. S2). For example, gluconapin,

Table 2
Molecular formulas, retention times (RT), *m/z* values ($[M-H]^-$), calculated and measured exact masses, mass errors (ppm), and double bond equivalents (DBE) for glucosinolate standards analyzed by UHPLC-DAD-HESI-Q-Orbitrap-MS.

Trivial name	Molecular formula	RT (min)	*m/z* $[M-H]^-$	Exact mass (calculated)	Exact mass (measured)	Error (ppm)	DBE
Gluconapin	$C_{11}H_{19}NO_9S_2$	2.03	372.04246	373.05013	373.04974	−1.037	3
Glucoraphanin	$C_{12}H_{23}NO_{10}S_3$	1.32	436.04109	437.04842	437.04837	−0.094	2
Glucolepidiin	$C_9H_{17}NO_9S_2$	0.85	346.02698	347.03448	347.03426	−0.623	2
Glucoarabin	$C_{17}H_{33}NO_{10}S_3$	3.89	506.11887	507.12667	507.12615	−1.011	2
Glucobrassicanapin	$C_{12}H_{21}NO_9S_2$	2.71	386.05825	387.06578	387.06553	−0.637	3
Glucoberteroin	$C_{13}H_{25}NO_9S_3$	3.65	434.06152	435.06915	435.06880	−0.799	2
Epiprogoitrin	$C_{11}H_{19}NO_{10}S_2$	1.15	388.03779	389.04504	389.04507	0.076	3
Glucocheirolin	$C_{11}H_{21}NO_{11}S_3$	1.05	438.02023	439.02768	439.02751	−0.378	2
Glucoiberin	$C_{11}H_{21}NO_{10}S_3$	0.85	422.02538	423.03277	423.03266	−0.240	2
Progoitrin	$C_{11}H_{19}NO_{10}S_2$	1.05	388.03760	389.04504	389.04488	−0.413	3
Glucocamelinin	$C_{18}H_{35}NO_{10}S_3$	4.46	520.13464	521.14232	521.14192	−0.753	2
Glucoraphenin	$C_{12}H_{21}NO_{10}S_3$	1.35	434.02515	435.03277	435.03243	−0.763	3
Glucoerucin	$C_{12}H_{23}NO_9S_3$	2.97	420.04615	421.05350	421.05343	−0.158	2
Sinigrin	$C_{10}H_{17}NO_9S_2$	1.20	358.02731	359.03448	359.03459	0.319	3
Homoglucocamelinin	$C_{19}H_{37}NO_{10}S_3$	5.04	534.15082	535.15797	535.15810	0.259	2
Glucomoringin	$C_{20}H_{29}NO_{14}S_2$	2.14	570.09520	571.10295	571.10248	−0.823	7
Glucolimnanthin	$C_{15}H_{21}NO_{10}S_2$	3.24	438.05310	439.06069	439.06038	−0.709	6
Gluconasturtiin	$C_{15}H_{21}NO_9S_2$	3.65	422.05863	423.06578	423.06591	0.318	6
Glucotropaeolin	$C_{14}H_{19}NO_9S_2$	2.89	408.04290	409.05013	409.05018	0.133	6
Sinalbin	$C_{14}H_{19}NO_{10}S_2$	1.82	424.03770	425.04504	425.04498	−0.142	6
4-Methoxyglucobrassicin	$C_{17}H_{22}N_2O_{10}S_2$	3.81	477.06400	478.07159	478.07128	−0.649	8
Neoglucobrassicin	$C_{17}H_{22}N_2O_{10}S_2$	4.45	477.06404	478.07159	478.07132	−0.565	8
Glucobrassicin	$C_{16}H_{20}N_2O_9S_2$	3.23	447.05331	448.06103	448.06059	−0.973	8

glucolepidiin, glucobrassicanapin, epiprogoitrin, glucoiberin, progoitrin, and sinigrin exhibited maximum responses at CVs of 40 V for *m/z* 275 and 259, respectively, while their responses at 60 V still exceeded 80% of the maximal response. These compounds were among the smallest in molecular weight (Table 2), except for glucoiberin. For *m/z* 97, only one compound deviated from the optimum CV of 60 V, yet still achieved 97% response at 60 V. For *m/z* 96, most compounds exhibited optimal CVs between 60 and 80 V, except for homoglucocamelinin and glucomoringin, the highest molecular weight compounds (Table 1), which still showed high abundance at 80 V. For *m/z* 80, a CV of 110 V was selected, as the highest signals were observed between 100 and 120 V, and a CV of 65 V was initially selected for *m/z* 75 based on the optimization curve (Fig. S2).

Collision energy (CE) optimization was done for *m/z* 241 and 259 with 10 product ions, 11 for *m/z* 275, and two for *m/z* 96 and 97. For the latter two, only *m/z* 80 and 64 were available. However, the *m/z* 64 product ion transitions were removed due to low abundance. Similarly, although the *m/z* 75 and 80 precursor ions showed high abundance in the CV optimization they were excluded after CE measurements revealed insufficient response for their product ions. In addition, several product ions for *m/z* 241, 259, and 275 precursors were excluded after initial MRM tests due to insufficient signal intensity. The remaining transitions (Table 3 and Fig. S3) were selected for validation measurements based on initial results indicating sensitivity and selectivity to glucosinolates. For compound-specific MRM, 5–10 product ions were tested for each precursor ion. Ultimately, ions exhibiting both high abundance and selectivity were selected, including *m/z* 97, 259, and neutral-loss fragments such as $[M-242-H]^-$, $[M-258-H]^-$, or $[M-336-H]^-$ ions (Table S1).

If small discrepancies were observed between optimized CVs (Fig. S2) or CEs (Fig. S3), different energy combinations were evaluated in the MRM method, and the energy settings yielding the highest signal intensity were selected. For instance, although *m/z* 259 and 275 had optimal CVs of 40 and 60 V, respectively, a compromise CV of 55 V yielded the highest overall response. Similarly, *m/z* 96 was finalized at 75 V after comparative testing.

It was noted that the qualitative/quantitative area ratios for precursor ion *m/z* 259 transitions did not stay constant throughout all compounds, where a qual/quan of 75 ± 23% standard deviation (SD) was observed. This indicated that the formation of *m/z* 139 and 97 is influenced by structure-dependent fragmentation, where structural features affect the fragmentation, resulting in different ion abundances. Phenomenon of inconsistency in the abundance of *m/z* 259 precursor ion has previously been reported by Rochfort et al. [20]. Therefore, the qual/quan ratios were grouped according to glucosinolate subgroups, side chain features, and molecular weight, allowing further comparison of structural properties to ion responses.

Table 3
Selected group-specific MRM precursor and product ions with optimized cone voltages (CVs), collision energies (CEs), and qualitative/quantitative (qual/quan) transition ratios.

Precursor ion (*m/z*)	Cone voltage (V)	Product ion (*m/z*)	Collision energy (eV)	Subgroup	qual/quan (area, %)*
95.9	75	79.9	15		
96.9	60	79.9	15		
259.0	55	**96.9**	20		
		139.0	20	Aliphatic[1]	47 ± 2
				Aliphatic[2]	112 ± 15
				Aliphatic[3]	75 ± 9
				Aromatic	59 ± 5
				Indole	81 ± 5

* = Ratio of qualitative to quantitative areas (qual/quan), along with their mean ± standard deviation.
Bolded product ion indicates the selected quantitative ion.
[1] = Alkyl/alkenyl.
[2] = Short-chain methylsulfinyl/methylsulfonyl.
[3] = Long-chain methylsulfinyl/hydroxyalkenyl/methylthio.

Analysis revealed that separating glucosinolates to subgroups correlated with distinct qual/quan ratios. Aromatic glucosinolates showed a qual/quan ratio of 59 ± 5% SD, while indole glucosinolates had a qual/quan of 81 ± 5% SD (Table 3). In contrast, aliphatic glucosinolates displayed greater variability, with an overall qual/quan ratio of 79 ± 27% SD. To better understand this variation, aliphatic compounds were further categorized based on their side chain structures into three subcategories. The first group included the four lowest molecular weight compounds, glucolepidiin, sinigrin, gluconapin, and glucobrassicanapin, all containing alkyl or alkenyl side chains. These compounds exhibited a consistent qual/quan ratio of 47 ± 2% SD. The

second group comprised compounds with short methylsulfinyl or methylsulfonyl chains, such as glucoraphanin, glucoiberin, glucocheirolin, and glucoraphenin, which showed a qual/quan ratio of 112 ± 15% SD. The third group consisted of compounds with methylthio, hydroxyalkenyl, or long-chain methylsulfinyl side chains, yielding a qual/quan ratio of 75 ± 9% SD (Table 3 and Fig. S5).

3.3. PRM method development

Group-specific parallel reaction monitoring (PRM) methods and compound-specific extracted ion chromatogram (EIC) methods were developed using a Thermo Fisher Scientific high-resolution hybrid Q-Orbitrap mass spectrometer. Similarly, for PRM, the compound-specific approach was developed to evaluate the performance of the group-specific methods relative to the compound-specific approach. Seven precursor ions (*m/z* 74.99101, 79.95737, 95.95228, 96.96011, 241.00237, 259.01293, and 274.99009) were initially selected for CID optimization, where fragments *m/z* 241, 259, and 275 showed no major compound-specific differences, with the highest responses observed at 40 eV (Fig. S4). For the EIC methods highest abundance ions, which were the deprotonated molecules in all cases, were selected for CID optimizations, where all compounds exhibited highest intensity at 0 eV.

Although PRM does not require normalized collision energy (NCE) optimization, it was performed to enhance the abundance of characteristic product ions. For *m/z* 241, the target fragments were *m/z* 79.96 and 96.96 (Fig. S6), for *m/z* 259 fragments at *m/z* 96.96 and 138.97 (Fig. S7), and for *m/z* 275 fragments at *m/z* 74.99 and 96.96 (Fig. S8). Because PRM allows simultaneous application of multiple collision energies, there was no need to select a single NCE suitable to all product ions. Therefore, after testing various NCE combinations three energies (20, 40, and 80 eV) were selected as they provided the most comprehensive spectral information with the highest abundances. The chosen settings also produced additional diagnostic ions, such as *m/z* 101.03, 168.98, and 198.99, enhancing the reliability of the identification. The lower molecular weight precursor ions, *m/z* 75, 80, 96, and 97, were excluded from further optimization due to insufficient fragmentation and lower selectivity toward glucosinolates. Also, various NCE combinations were tested to EIC methods, from which a combination of 30, 50, and 80 eV was selected to all methods.

3.4. Method validation

3.4.1. LOD, LOQ, and ULOQ

An 11-point dilution series was prepared between 100 µg/mL – 193 pg/mL to evaluate the LOD, LOQ, and ULOQ. The dilution series was made in two ways: one pure solution and one matrix-spiked. This approach also allowed assessment of matrix effects to LOD, LOQ, and ULOQ results. The LOD and LOQ were calculated based on the formulas shown in Section 2.6. Calibration curve linearity was evaluated by visual inspection and heteroscedasticity. Additionally, all the calibration curves that met linearity criteria exhibited a coefficient of determination (R^2) greater than 0.995. Glucoerucin showed substantially higher LOD and LOQ values, which could not be fully explained but were likely associated with solubility or stability limitations. Hence, glucoerucin was excluded from the method validation as the results were deemed unreliable.

The group-specific MRM methods demonstrated good sensitivity (Fig. 5). Of all the group-specific MRM methods, the lowest LODs were obtained with transitions *m/z* 95.9 > 79.9 and 96.9 > 79.9 (Fig. S9), with LODs ranging from 11.5 to 196.0 ng/mL and 16.4–156.3 ng/mL, respectively. The lowest LOD was observed for homoglucocamelinin with *m/z* 95.9 > 79.9 transition. However, the *m/z* 95.9 > 79.9 and 96.9 > 79.9 transitions lack selectivity for glucosinolates, requiring the selection of additional precursor ions. Hence, multiple transitions derived from precursor ions *m/z* 241, 259, and 275 were evaluated during method validations, but only two transition were ultimately selected to the final method. The additional transitions were rejected due to their poor detection limits, linear ranges, and/or overall analytical performance during method validation. The selected transitions were *m/z* 259.0 > 96.9 and 259.0 > 139.0, which exhibited LODs between 40.2–558.2 ng/mL and 18.1–230.3 ng/mL, respectively (Figs. 5 and S9A). ULOQ values varied by precursor ion, where the values for *m/z* 95.9 > 79.9 and 96.9 > 79.9 varied between 2.5–9.2 µg/mL, i.e., the fourth and fifth highest measurement points. The *m/z* 259.0 > 96.9 and 259.0 > 139.0 transitions exhibited ULOQ between 2.5 and 55 µg/mL (Fig. S9C).

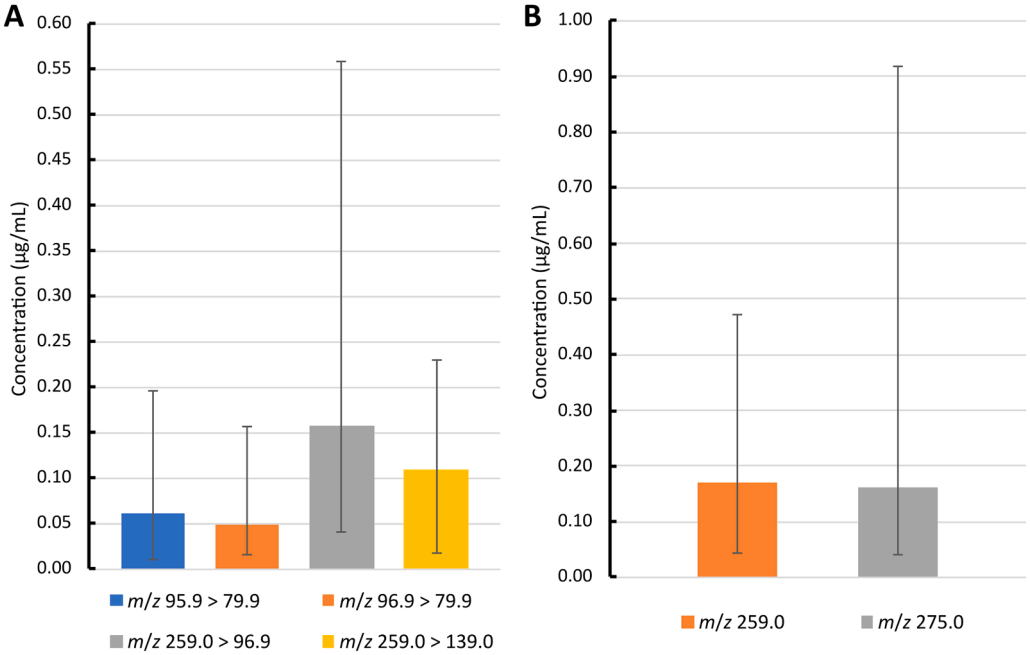

Fig. 5. Mean limits of detection (LODs) for group-specific MRM (A) and PRM (B) methods. Error bars indicate the lowest and highest LOD values obtained across all compounds.

Compound-specific MRM methods exhibited slightly lower LOD and LOQ values than group-specific methods (Fig.s S9 and S11). Each method included three transitions: *m/z* 96.9 as the quantitative ion and *m/z* 259.0 plus a characteristic neutral-loss ion for qualitative confirmation (Table S1). The LODs for the quantitative transitions ranged between 2.5 and 46.8 ng/mL, with the lowest LOD observed for glucoraphanin. The qualitative transitions LODs ranged from 8.9 to 139.0 ng/mL (Fig. S11A). ULOQs for compound-specific methods ranged from 0.7 to 25 μg/mL (Fig. S11C).

Matrix effects were evident in spiked samples, where LOD and LOQ values were generally higher. For example, the LODs for the *m/z* 96.9 > 79.9 transition varied substantially between individual compounds, ranging from 0.67-fold to 74-fold in matrix-spiked samples compared to pure solution sample, where compounds such as glucoraphanin, glucolepidiin, and epiprogoitrin showed similar or lower LODs in matrix-spiked samples (Fig. S10). For precursor ion *m/z* 259, the matrix effect was less pronounced, with LODs varying from 0.27-fold to 12-fold in matrix-spiked samples, confirming minimal impact on method performance in most cases. Compound-specific MRMs also exhibited higher LODs in matrix-spiked samples, except for sinigrin, which showed a slightly lower LOD in matrix-spiked sample (Figs. S11–S12). ULOQs in matrix-spiked samples were occasionally one or two points higher, partially explaining the increased calculated LOD and LOQ values. Additionally, some transitions did not exhibit linearity for certain compounds in matrix-spiked samples (Figs. S10E and S12E). Glucoberteroin also exhibited ULOQ around 100 μg/mL, which meant that the ULOQ may extend beyond the highest measured point; however, calibration points were restricted to 100 μg/mL due to the lack of necessity to measure higher concentrations.

Group-specific PRM methods produced results comparable to group-specific MRM. The lowest LODs were observed for *m/z* 259 with results ranging from 44.1 to 473.6 ng/mL, while *m/z* 275 LODs ranged from 40.3 to 917.2 ng/mL (Figs. 5 and S13). For these precursor ions the ULOQs ranged between 8 and 51 μg/mL. Compound-specific EIC methods demonstrated the highest overall sensitivity, with calculated LODs ranging from 14.8 to 336.0 ng/mL and ULOQs between 8 and 25 μg/mL (Fig. S15). However, visual inspection of the chromatograms suggested even better sensitivity, with LODs corresponding to the first through third lowest measurement points (0.2–7.3 ng/mL). This discrepancy indicates that the LOD/LOQ calculation methods used for MRM and PRM is not fully applicable to EIC methods.

The impact of matrix effects on LODs, LOQs, and ULOQs was more pronounced for PRM than for MRM methods (Figs. S10 and S14). For example, the LODs for precursor ion *m/z* 259 changed by 0.72-fold to 34-fold. Similarly, ULOQ values for *m/z* 259 increased by one or two calibration points, and for *m/z* 275, approximately half of the compounds failed to exhibit a linear range. Additionally, many compounds exhibited a ULOQ near 100 μg/mL indicating that the true ULOQ may likely extend beyond that point. In the case of glucoraphenin with *m/z* 275 precursor, matrix interference was so severe that LOD, LOQ, and ULOQ could not be determined (Fig. S16). This was attributed to co-elution of gallic acid (*m/z* 169) with glucoraphenin in the matrix-spiked plant extract, indicating that precursor ion *m/z* 275 is less suitable for complex matrices. The compound-specific EIC methods showed a similar trend, with calculated LOD varying by a factor of 0.27 to 38 (Fig. S16) in matrix-spiked samples compared to pure solution samples. However, for the majority of compounds, LOD and LOQ values in matrix-spiked samples remained consistent with those obtained from pure solution sample, indicating that EIC methods were largely unaffected by matrix interference from the plant extract mixture. The ULOQs either remained unchanged or showed minor increases.

Visual inspection of LODs generally aligned with calculated values, with only minor discrepancies. The largest differences occurred when ULOQs were very high, which inflated calculated LODs relative to those observed visually. This was particularly evident in transitions where high ULOQs coincided with transitions that otherwise produced low LODs. In most cases, however, calculated LODs closely matched visual estimates, confirming the suitability of the applied formulas, except for EIC methods. For instance, when the visually determined LOD corresponded to the sixth calibration point, the calculated LOD typically fell between the sixth and seventh point or closely approximated the sixth.

3.4.2. Repeatability

Repeatability of the MRM methods was assessed at 1 μg/mL using ten replicate injections. The group-specific MRM methods showed mean relative standard deviations (RSDs) of 8.8% for *m/z* 96, 7.2% for *m/z* 97, and 9.8% for *m/z* 259 (Figs. 6 and S17A). Results for individual compounds were generally consistent with these averages, ranging from 3.9% to 18.6% for *m/z* 96, 2.8–11.3% for *m/z* 97, and 5.4–16.3% for *m/z* 259. In some cases, elevated RSDs were attributed to the repeatability's concentration being near the LOQ values, where greater variability is expected. For compound-specific MRM, the RSDs varied between 0.7–4.4% for quantitative transitions and 1.2–10.6% and 1.1–8.9% for the first and second qualitative transitions, respectively. Additionally, to compare the repeatability of MRMs, UV detection at 230 nm was measured at 230 nm, which showed a mean RSD of 2.6%, with results ranging from 1.3% to 4.1% (Fig. S17B). Overall, the results showed that the selected group- and compound-specific methods demonstrated good repeatability.

Repeatability of PRM and EIC methods was evaluated at 2 μg/mL with ten replicate injections. A slightly higher concentration was selected for the high-resolution instrument due to observation that our DAD coupled with the HR-MS produced approximately 25% lower signal intensity compared to our eλ DAD coupled with the TQ-MS system. The EIC methods yielded an average RSD of 2.5%, with results ranging from 1.2% to 8.2%, where areas the PRM methods exhibited mean RSD of 2.3% for *m/z* 259 and 2.7% for *m/z* 275 (Figs. 6 and S18). The precision values for individual compounds varied between 1.0% and 10.9% for precursor *m/z* 259 and between 1.0% and 10.3% for precursor *m/z* 275. UV detection at 230 nm averaged 2.7% precision, excluding six compounds that could not be detected due to the lower sensitivity of the DAD coupled to the HR-MS (Fig. S18). The highest PRM RSD was observed for sinigrin (7.6–10.9% depending on precursor ion), whereas its UV response RSD was only 1.0%. The elevated RSD was attributed to a single outlier that fell 2.5–2.7 SD below the mean, possibly caused by transient ionization instability. Still, these results confirm that both group- and compound-specific methods using PRM and EIC approaches exhibit high repeatability under the tested conditions.

3.4.3. Matrix effect

Matrix effects were calculated from high-concentration range as the average response ratio of the four highest calibration points (approximately 8–100 μg/mL) and from medium-concentration range, i.e., from the fifth highest measurement point approximately at 3 μg/mL. The standards were added to the plant extract mixture post-extraction. The plant species selected for the matrix effect assessments were chosen to represent complex glucosinolate-free plant matrices. The selection was based on published information and prior knowledge of these species' chemical diversity [59]. This was further verified through comprehensive full scan MS and UV analyses of the samples.

Group-specific MRM methods showed signal suppression and enhancement in matrix-spiked samples. In the high-concentration range, matrix effects ranged from 73% to 120% for *m/z* 96, 73–117% for *m/z* 97, and 58–104% for *m/z* 259 (Fig. 6 and Table S2). In the medium-concentration range, variability increased, with matrix effects spanning 68–140% (*m/z* 96), 74–174% (*m/z* 97), and 47–126% (*m/z* 259) (Fig. 6 and Table S3). For glucoberteroin, matrix effects were calculated as an average of the three highest measurement points, i.e., approximately 25–100 μg/mL, due strong interference below this range, likely caused by co-eluting compounds such as caffeic acid, ellagitannin, and galloyl glucose derivatives.

Compound-specific MRM methods showed matrix effects ranging

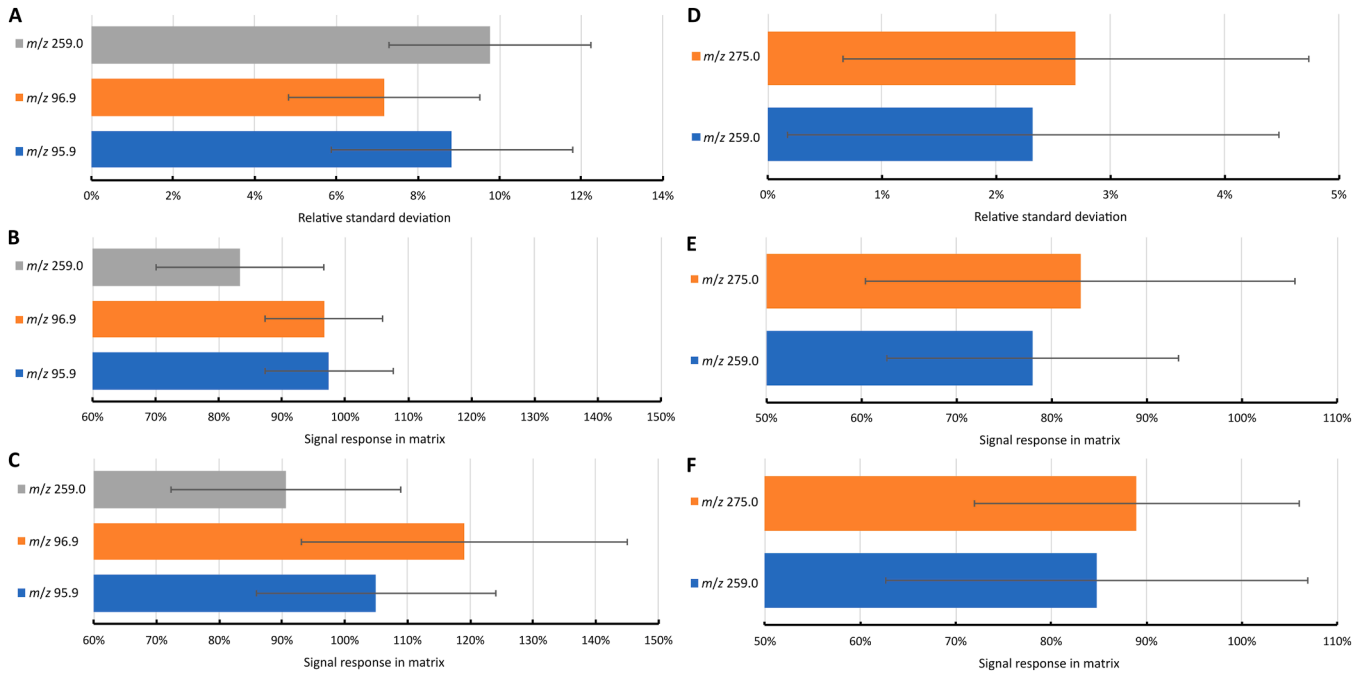

Fig. 6. Mean repeatability (A, D) and matrix effects at high (B, E) and medium (C, F) concentration ranges for group-specific MRM (A–C) and PRM (D–E) methods. Error bars represent the standard deviation. In panel F, *m/z* 275 includes only 5 compounds, and for *m/z* 259 two compounds lacked sufficient signal for matrix effect calculation.

from 66% to 107%, 49–109%, and 62–108% in high-concentration range for quantitative, first qualitative, and second qualitative transitions, respectively (Table S4). Medium-concentration range results again exhibited slightly increased variability, where matrix effects varied between 53% and 133% for quantitative transitions, 39% to 129% for first qualitative transitions, and 47% to 130% for second qualitative transitions (Table S5). Notably, matrix effects for glucoberteroin could not be determined in the medium-concentration range due to signal interference. Also, 4-methoxyglucobrassicin exhibited strong signal suppression likely due to co-elution with quinic acid (*m/z* 353, caffeoyl quinic acid), ellagitannin (*m/z* 935, casuarictin), and flavonol derivatives (*m/z* 609, quercetin rutinoside), identified via internal spectral library.

Group-specific PRM methods displayed greater ion suppression, where matrix effects ranged from 44% to 103% for *m/z* 259 and 32–123% for *m/z* 275 in high-concentration range, and in medium-concentration range from 34% to 146% for *m/z* 259 and 67–112% for *m/z* 275 (Fig. 6 and Tables S6–S7). Glucoberteroin again exhibited significant interference from false positives. Therefore, its matrix effect at the high-concentration range was calculated over 25–100 µg/mL rather than 8–100 µg/mL. Additionally, false positives with *m/z* 275 severely impacted detection in the medium-concentration range, especially for early-eluting compounds like glucoraphenin, which co-eluted close to a false positive peak at 1.2 min, obscuring the analyte signal beyond the second highest calibration point. Consequently, matrix effects for *m/z* 275 were calculated using only the top three calibration points. Compound-specific EIC methods demonstrated lower matrix effects compared to PRM methods, ranging between 65% and 113% in high-concentration range and 67% to 122% in medium-concentration range (Tables S6–S7).

As expected, ion suppression and enhancement were observed in matrix-spiked samples, with suppression largely attributed to co-eluting compounds. Although PRM methods exhibited greater variability, both PRM and MRM approaches remained suitable for plant matrices, with average matrix effects above 75% for *m/z* 259 and around 100% or slightly higher for *m/z* 96 and 97 across both concentration ranges. While a 20% signal reduction is generally considered acceptable, some transitions exhibited significantly stronger suppression, indicating pronounced matrix interference. To mitigate matrix effects, sample clean-up or changing chromatographic conditions could help reduce co-eluting compounds [60]. Additionally, the use of internal standards [61] and/or sample dilution [62] could further correct for matrix effects and enhance quantification accuracy. However, matrix effects are also compound- and matrix-dependent and may be less pronounced in real samples where target compounds are naturally present. This was evident in method application, where PRM methods precursor *m/z* 275 showed less false positives in glucosinolate containing plant extracts compared to the matrix-spiked sample.

3.4.4. *Selectivity and specificity*

Selectivity and specificity were evaluated using glucosinolate-free extracts from various plant species (Section 2.2) to identify potential false positives. Group-specific MRM methods incorporated multiple transitions, enabling verification through transition ratios (Table 3 and Fig. S5) [46]. For PRM, precursor ions were required to produce characteristic product ions for confirmation (Figs. S6–S8). This approach ensured that any non-glucosinolate compounds could be identified by deviations in transition ratios or absence of diagnostic fragments.

Overall, the group-specific MRM methods exhibited only a few false positives, most of which were low in intensity, typically corresponding to signal levels near the LOD or LOQ values. A consistent signal at ~0.65 min for the transition *m/z* 96.9 > 79.9 was observed in both plant extract mixtures and independent of concentration and was attributed to an instrument artifact. Since no glucosinolates elute at this retention time, this did not affect detection. Additionally, low-level false positives were observed for *m/z* 96.9 > 79.9 and 95.9 > 79.9 at the same retention time, but these did not coincide with either *m/z* 259 transitions. Furthermore, a few low intensity false positives were noted for transition *m/z* 96.9 > 79.9. One high-abundance false positive was observed for *m/z* 259.0 > 96.9, with the highest abundance ions being *m/z* 371, 477, 599, 285, and 991, and UV spectrum suggesting a flavonol derivative [63]. Importantly, no compound triggered false positives across all transitions in the selected MRM methods, confirming their effectiveness in plant matrices. Compound-specific MRM methods did not produce

false positives, as expected, due to their high selectivity and specificity, primarily resulting from narrow retention time windows but also from the use of higher molecular weight precursor ions compared to group-specific methods.

PRM methods exhibited more frequent false positives, especially for the *m/z* 275 precursor ion. It was noted that the false positives of precursor *m/z* 275, mostly at early retention times, were likely contributed to elevated LOD, LOQ, and ULOQ values in matrix-spiked samples (Fig. S15). However, these product ion spectra differed from those of authentic glucosinolates. In contrast, precursor *m/z* 259 showed only a few false positives, none matching glucosinolate fragmentation patterns. Compound-specific EIC methods did not exhibit false positive signals within their defined retention time windows. Overall, while isolated precursor ions produced false positives, no single compound triggered false positives for both *m/z* 259 and 275, nor did any show characteristic product ions for *m/z* 259 (Fig. S7), confirming the selectivity and suitability of the group-specific PRM methods for plant matrices.

3.5. Application of the methods

Beyond selectivity testing, the methods were applied to 20 plant species with a high likelihood of containing glucosinolates, primarily from the Brassicaceae family. Glucosinolates were detected in 19 species, with the exception of *Camelina sativa* leaves, consistent with literature indicating their presence being confined to seeds [16,43]. Group-specific methods proved their effectiveness in rapid screening, while compound-specific methods demonstrated slightly better sensitivity.

A total of 324 glucosinolates were detected, corresponding to 51 distinct compounds identified based on literature and MS/MS fragmentation patterns (Table S8). Several additional compounds were also observed, likely aliphatic glucosinolates, but could not be fully characterized. Structural confirmation was supported by TopN analyses and diagnostic fragment verification. Identified compounds were categorized into four identification (ID) levels based on the framework proposed by Sumner et al. [64]. Level 1 indicates the highest confidence in compound characterization, while level 4 reflects the lowest. To be classified as level 1, a compound required supporting data, such as accurate mass measurements combined with MS/MS spectra or a match in both retention time and mass spectra with in-house reference standards. In cases where such data were not available but the compound had been previously reported in the literature, it was assigned to ID level 2.

The number of glucosinolates varied significantly between species, ranging from 27 found in *Arabis caucasica* to only two in *Draba hispanica*, the latter detectable only by compound-specific MRM and EIC due to low abundance (Table S8). Isomeric compounds, e.g., 10-(methylsulfonyl)decyl glucosinolate, were identified in *Arabis caucasica*, showing similar fragmentation patterns and positive signals across all methods but differing in retention time. The methods also revealed the presence of previously characterized glucosinolates in new species, including 11-(methylsulfonyl)decyl glucosinolate in *Brassica nigra* and n-heptyl glucosinolate in *Brassica napus*. Moreover, two glucoarabin isomers were found in *Arabis caucasica*, corresponding to probable side chain branching of the structure. These results underscore the utility of group-specific methods in expanding the phytochemical diversity of glucosinolates across plant species.

While many species exhibited similarities in glucosinolate contents, particularly within the same genus, both qualitative and quantitative differences were evident. Even cultivars of *Brassica juncea* and *Brassica rapa* displayed distinct chromatographic fingerprints with the group-specific methods (Fig. 7). For instance, sinigrin, eluting at 1.15 min, was only detected in *Brassica rapa* with the group-specific methods (Fig. 7A), although compound-specific methods detected it across all *Brassica rapa* cultivars. Similar differences were observed in *Brassica juncea*, where gluconapin eluting around 2 min showed higher abundance in the 'Bloody Mary' cultivar compared to other cultivars (Fig. 7B).

Minor differences between MRM and PRM methods were also

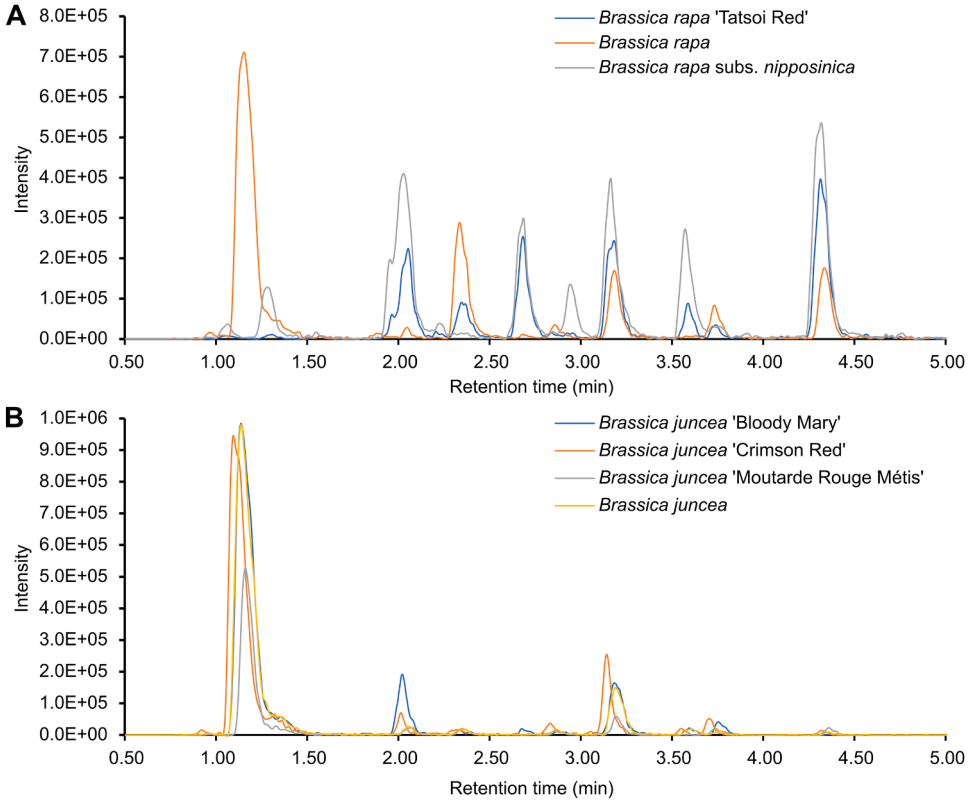

Fig. 7. Group-specific MRM chromatographic fingerprints of *m/z* 95.9 > 79.9 transition across cultivars of *Brassica rapa* (A) and *Brassica juncea* (B).

apparent (Fig. 8), with MRM enabling rapid detection via selective transitions, and PRM enabling accurate characterization. Although PRM methods showed higher LOD and LOQ values during method validation, the precursor ions *m/z* 259 and 275 performed well across all samples, approaching the sensitivity levels of MRM methods based on visual assessment. Minor sensitivity differences between MRM and PRM were evident through the *m/z* 96 and 97 transitions, which were the only group-specific methods capable of detecting otherwise undetectable low-abundance compounds. Importantly, PRM methods did not produce false positives, especially with the *m/z* 275 precursor ion, showing high specificity in these plant extracts.

4. Conclusions

This study presents two complementary strategies for developing targeted, group-specific MS/MS methods for glucosinolates. These approaches can be adapted to other MS/MS platforms, enabling rapid screening of entire compound classes or specific subgroups. The selected methods achieved robust detection and quantification of glucosinolates with good linearity, reasonable matrix interference, and most of all high selectivity. While high-resolution PRM offers superior mass accuracy, it is limited by slower acquisition speed. Therefore, MRM remains the preferred tool for routine screening and quantification, with PRM serving as a confirmatory method for accurate mass verification and fragmentation spectrum. Despite variability in the group-specific MRM qual/quan ratios of *m/z* 259 transitions, its strong sensitivity, high selectivity, and ability to distinguish glucosinolate subgroups supported its inclusion. The group-specific MRM methods combine low detection limits via *m/z* 96 and 97 with selectivity and specificity through *m/z* 259 precursor ion.

For PRM, only one method could be parallel with full scan MS in quantitative purposes due to Orbitrap's scan speed limitations. Hence, two PRM workflows were established: (i) a quantitative method utilizing *m/z* 259 with full scan MS and (ii) a qualitative method combining two PRM methods (*m/z* 259 and 275) alongside full scan MS. Although the precursor *m/z* 275 showed strong matrix effects and limited selectivity to glucosinolates, it can be used as a confirming ion enhancing detection reliability; however, the *m/z* 259 should remain as the primary ion. The inclusion of *m/z* 275 alongside *m/z* 259 proved beneficial during method application, contributing to improved robustness and faster detection.

Overall, this work demonstrates that group-specific MS/MS methods offer significant potential for rapid and selective analysis of structurally related compounds without sacrificing method performance. As characteristic fragments for many compound classes are well documented, broader adoption of such strategies could accelerate the characterization of chemical diversity in plants and other complex matrices.

Declaration of generative AI and AI-assisted technologies in the manuscript preparation process

During the preparation of this work the author(s) used Microsoft Copilot exclusively in order to enhance the readability of the text. After using this tool/service, the author(s) reviewed and edited the content as needed and take(s) full responsibility for the content of the published article.

CRediT authorship contribution statement

Ville Fock: Writing – original draft, Visualization, Validation, Methodology, Investigation, Formal analysis, Data curation. **Niko Luntamo:** Writing – review & editing, Supervision, Methodology, Conceptualization. **Juha-Pekka Salminen:** Writing – review & editing, Supervision, Resources, Project administration, Methodology, Conceptualization.

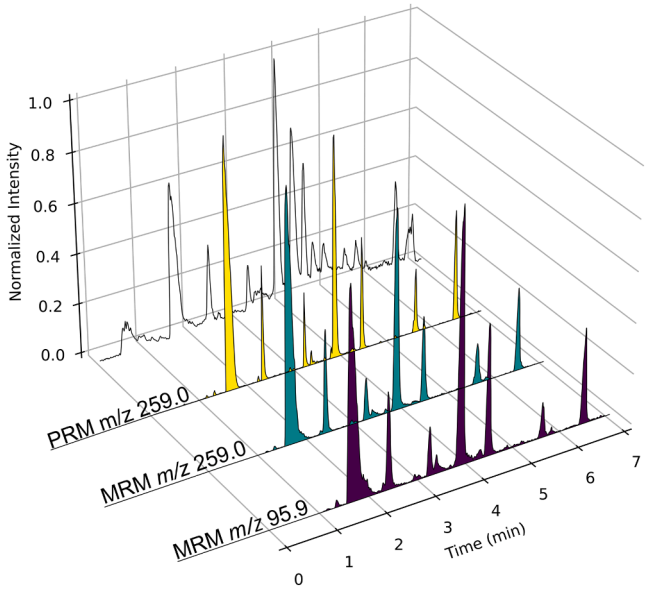

Fig. 8. Group-specific MRM and PRM chromatograms illustrated with *Arabis caucasica*, where the background signal corresponds to negative ionization full scan MS.

Declaration of competing interest

The authors declare that they have no known competing financial interests or personal relationships that could have appeared to influence the work reported in this paper.

Acknowledgments

This project was supported by grant from the Magnus Ehrnrooth foundation. I would like to express my gratitude to Marica Engström for her support in reviewing and editing the manuscript. I also want to thank all members of the Natural Chemistry Research Group (NCRG) for their support.

Supplementary materials

Supplementary material associated with this article can be found, in the online version, at doi:10.1016/j.chroma.2026.466913.

Data availability

Data will be made available on request.

References

[1] S. Baldelli, M. Lombardo, A. D'Amato, S. Karav, G. Tripodi, G. Aiello, Glucosinolates in Human health: metabolic pathways, bioavailability, and potential in chronic disease prevention, Foods 14 (2025) 912, https://doi.org/10.3390/FOODS14060912.

[2] S.H. Choi, S. Park, Y.P. Lim, S.J. Kim, J.T. Park, G. An, Metabolite profiles of glucosinolates in cabbage varieties (*Brassica oleracea* var. *capitata*) by season, color, and tissue position, Hortic. Env. Biotechnol. 55 (2014) 237–247, https://doi.org/10.1007/S13580-014-0009-6.

[3] R.N. Bennett, F.A. Mellon, N. Foidl, J.H. Pratt, M.S. Dupont, L. Perkins, P.A. Kroon, Profiling glucosinolates and phenolics in vegetative and reproductive tissues of the multi-purpose trees *Moringa oleifera* L. (Horseradish tree) and *Moringa stenopetala* L, J. Agric. Food Chem. 51 (2003) 3546–3553, https://doi.org/10.1021/jf0211480.

[4] R. Mithen, K. Faulkner, R. Magrath, P. Rose, G. Williamson, J. Marquez, Development of isothiocyanate-enriched broccoli, and its enhanced ability to induce phase 2 detoxification enzymes in mammalian cells, Theor. Appl. Genet. 106 (2003) 727–734, https://doi.org/10.1007/S00122-002-1123-X.

[5] I. Blažević, S. Montaut, F. Burčul, C.E. Olsen, M. Burow, P. Rollin, N. Agerbirk, Glucosinolate structural diversity, identification, chemical synthesis and metabolism in plants, Phytochemistry 169 (2020) 112100, https://doi.org/10.1016/J.PHYTOCHEM.2019.112100.

[6] N. Agerbirk, C.E. Olsen, Glucosinolate structures in evolution, Phytochemistry 77 (2012) 16–45, https://doi.org/10.1016/J.PHYTOCHEM.2012.02.005.

[7] D.B. Clarke, Glucosinolates, structures and analysis in food, Anal. Methods 2 (2010) 301–416, https://doi.org/10.1039/b9ay00280d.

[8] C.E. Olsen, X.C. Huang, C.I.C. Hansen, D. Cipollini, M. Ørgaard, A. Matthes, F. Geu-Flores, M.A. Koch, N. Agerbirk, Glucosinolate diversity within a phylogenetic framework of the tribe Cardamineae (Brassicaceae) unraveled with HPLC-MS/MS and NMR-based analytical distinction of 70 desulfoglucosinolates, Phytochemistry 132 (2016) 33–56, https://doi.org/10.1016/J.PHYTOCHEM.2016.09.013.

[9] T. Wang, H. Liang, Q. Yuan, Separation of sinigrin from Indian mustard (*Brassica juncea* L.) seed using macroporous ion-exchange resin, Korean J. Chem. Eng. 29 (2012) 396–403, https://doi.org/10.1007/s11814-011-0175-5.

[10] B. Matthäus, H. Luftmann, Glucosinolates in members of the Family Brassicaceae: separation and identification by LC/ESI-MS-MS, J. Agric. Food Chem. 48 (2000) 2234–2239, https://doi.org/10.1021/JF991306W.

[11] M. Francisco, D.A. Moreno, M.E. Cartea, F. Ferreres, C. García-Viguera, P. Velasco, Simultaneous identification of glucosinolates and phenolic compounds in a representative collection of vegetable *brassica rapa*, J. Chromatogr. A 1216 (2009) 6611–6619, https://doi.org/10.1016/J.CHROMA.2009.07.055.

[12] K. Grosser, N.M. van Dam, A straightforward method for glucosinolate extraction and analysis with high-pressure liquid chromatography (HPLC), J. Vis. Exp. 2017 (2017) 55425, https://doi.org/10.3791/55425.

[13] P. Franco, S. Spinozzi, E. Pagnotta, L. Lazzeri, L. Ugolini, C. Camborata, A. Roda, Development of a liquid chromatography–electrospray ionization–tandem mass spectrometry method for the simultaneous analysis of intact glucosinolates and isothiocyanates in Brassicaceae seeds and functional foods, J. Chromatogr. A 1428 (2016) 154–161, https://doi.org/10.1016/J.CHROMA.2015.09.001.

[14] J.B. Bialecki, J. Ruzicka, C.S. Weisbecker, M. Haribal, A.B. Attygalle, Collision-induced dissociation mass spectra of glucosinolate anions, J. Mass Spectrom. 45 (2010) 272–283, https://doi.org/10.1002/JMS.1711.

[15] S. Millán, M.C. Sampedro, P. Gallejones, A. Castellón, M.L. Ibargoitia, M. A. Goicolea, R.J. Barrio, Identification and quantification of glucosinolates in rapeseed using liquid chromatography-ion trap mass spectrometry, Anal. Bioanal. Chem. 394 (2009) 1661–1669, https://doi.org/10.1007/S00216-009-2823-8.

[16] D. Yuan, Y.Y. Shim, J. Shen, P.D. Jadhav, V. Meda, M.J.T. Reaney, Distribution of glucosinolates in camelina seed fractions by HPLC-ESI-MS/MS, Eur. J. Lipid Sci. Technol. 119 (2017) 1600040, https://doi.org/10.1002/EJLT.201600040.

[17] F.A. Mellon, R.N. Bennett, B. Holst, G. Williamson, Intact glucosinolate analysis in plant extracts by programmed cone voltage electrospray LC/MS: performance and comparison with LC/MS/MS methods, Anal. Biochem. 306 (2002) 83–91, https://doi.org/10.1006/ABIO.2002.5677.

[18] L.E. Mocniak, K.R. Elkin, S.L. Dillard, R.B. Bryant, K.J. Soder, Building comprehensive glucosinolate profiles for brassica varieties, Talanta 251 (2023) 123814, https://doi.org/10.1016/j.talanta.2022.123814.

[19] T.R.I. Cataldi, A. Rubino, F. Lelario, S.A. Bufo, Naturally occurring glucosinolates in plant extracts of rocket salad (*Eruca sativa* L.) identified by liquid chromatography coupled with negative ion electrospray ionization and quadrupole ion-trap mass spectrometry, Rapid. Commun. Mass Spectrom. 21 (2007) 2374–2388, https://doi.org/10.1002/RCM.3101.

[20] S.J. Rochfort, V.C. Trenerry, M. Imsic, J. Panozzo, R. Jones, Class targeted metabolomics: ESI ion trap screening methods for glucosinolates based on MSn fragmentation, Phytochemistry 69 (2008) 1671–1679, https://doi.org/10.1016/J.PHYTOCHEM.2008.02.010.

[21] G. Bianco, R. Pascale, F. Lelario, S.A. Bufo, T.R.I. Cataldi, The Investigation of Glucosinolates by Mass Spectrometry, Springer Science and Business Media B.V, 2017, https://doi.org/10.1007/978-3-319-25462-3_12.

[22] H.J. Kim, M.J. Lee, M.H. Jeong, J.E. Kim, Identification and quantification of glucosinolates in Kimchi by liquid chromatography-electrospray tandem mass spectrometry, Int. J. Anal. Chem. 2017 (2017), https://doi.org/10.1155/2017/6753481.

[23] M. Ishida, I. Chiba, Y. Okuyama, Y. Takahata, N. Kaizuma, Separation and identification of desulfoglucosinolates in Japanese rapessed by LC/APCI-MS, Jpn. Agric. Res. Q 31 (1997) 73–80.

[24] R.P. Tolrà, R. Alonso, C. Poschenrieder, D. Barceló, J. Barceló, Determination of glucosinolates in rapeseed and *Thlaspi caerulescens* plants by liquid chromatography–atmospheric pressure chemical ionization mass spectrometry, J. Chromatogr. A 889 (2000) 75–81, https://doi.org/10.1016/S0021-9673(00)00373-3.

[25] V.P. Thinh Nguyen, J. Stewart, M. Lopez, I. Ioannou, F. Allais, Glucosinolates: natural occurrence, biosynthesis, accessibility, isolation, structures, and biological activities, Molecules. 25 (2020), https://doi.org/10.3390/MOLECULES25194537.

[26] Q. Tian, R.A. Rosselot, S.J. Schwartz, Quantitative determination of intact glucosinolates in broccoli, broccoli sprouts, Brussels sprouts, and cauliflower by high-performance liquid chromatography–electrospray ionization–tandem mass spectrometry, Anal. Biochem. 343 (2005) 93–99, https://doi.org/10.1016/J.AB.2005.04.045.

[27] K.-C. Lee, M.-W. Cheuk, W. Chan, A.W.-M. Lee, Z.-Z. Zhao, Z.-H. Jiang, Z. Cai, Determination of glucosinolates in traditional Chinese herbs by high-performance liquid chromatography and electrospray ionization mass spectrometry, Anal. Bioanal. Chem. 386 (2006) 2225–2232, https://doi.org/10.1007/S00216-006-0882-7.

[28] Z. Cai, C.Y. Cheung, W.T. Ma, W.M. Au, X.Y. Zhang, A. Lee, Determination of two intact glucosinolates in vegetables and Chinese herbs, Anal. Bioanal. Chem. 378 (2004) 827–833, https://doi.org/10.1007/S00216-003-2335-X.

[29] M. Maldini, S. Baima, G. Morelli, C. Scaccini, F. Natella, A liquid chromatography-mass spectrometry approach to study "glucosinoloma" in broccoli sprouts, J. Mass Spectrom. 47 (2012) 1198–1206, https://doi.org/10.1002/JMS.3028.

[30] M. Gratacós-Cubarsí, A. Ribas-Agustí, J.A. García-Regueiro, M. Castellari, Simultaneous evaluation of intact glucosinolates and phenolic compounds by UPLC-DAD-MS/MS in *brassica oleracea* L. var. *Botrytis*, Food Chem. 121 (2010) 257–263, https://doi.org/10.1016/J.FOODCHEM.2009.11.081.

[31] A.M. Ares, M.J. Nozal, J.L. Bernal, J. Bernal, Optimized extraction, separation and quantification of twelve intact glucosinolates in broccoli leaves, Food Chem. 152 (2014) 66–74, https://doi.org/10.1016/J.FOODCHEM.2013.11.125.

[32] F. Lelario, G. Bianco, S.A. Bufo, T.R.I. Cataldi, Establishing the occurrence of major and minor glucosinolates in Brassicaceae by LC–ESI-hybrid linear ion-trap and fourier-transform ion cyclotron resonance mass spectrometry, Phytochemistry 73 (2012) 74–83, https://doi.org/10.1016/J.PHYTOCHEM.2011.09.010.

[33] N. Fabre, V. Poinsot, L. Debrauwer, C. Vigor, J. Tulliez, I. Fourasté, C. Moulis, Characterisation of glucosinolates using electrospray ion trap and electrospray quadrupole time-of-flight mass spectrometry, Phytochem. Anal. 18 (2007) 306–319, https://doi.org/10.1002/PCA.983.

[34] R.N. Bennett, F.A. Mellon, N.P. Botting, J. Eagles, E.A.S. Rosa, G. Williamson, Identification of the major glucosinolate (4-mercaptobutyl glucosinolate) in leaves of *Eruca sativa* L. (salad rocket), Phytochemistry 61 (2002) 25–30, https://doi.org/10.1016/S0031-9422(02)00203-0.

[35] M.F. Fernández-León, A.M. Fernández-León, M. Lozano, M.C. Ayuso, D. González-Gómez, Identification, quantification and comparison of the principal bioactive compounds and external quality parameters of two broccoli cultivars, J. Funct. Foods. 4 (2012) 465–473, https://doi.org/10.1016/J.JFF.2012.02.005.

[36] L. Song, P.J. Thornalley, Effect of storage, processing and cooking on glucosinolate content of *Brassica* vegetables, Food Chem. Toxicol. 45 (2007) 216–224, https://doi.org/10.1016/J.FCT.2006.07.021.

[37] S.Y. Kim, J. Yang, Y.M. Dang, J.H. Ha, Effect of fermentation stages on glucosinolate profiles in kimchi: quantification of 14 intact glucosinolates using ultra-performance liquid chromatography-tandem mass spectrometry, Food Chem. 15 (2022) 100417, https://doi.org/10.1016/J.FOCHX.2022.100417.

[38] M. Thomas, A. Badr, Y. Desjardins, A. Gosselin, P. Angers, Characterization of industrial broccoli discards (*Brassica oleracea* var. *italica*) for their glucosinolate, polyphenol and flavonoid contents using UPLC MS/MS and spectrophotometric methods, Food Chem. 245 (2018) 1204–1211, https://doi.org/10.1016/J.FOODCHEM.2017.11.021.

[39] A.L. Capriotti, C. Cavaliere, G. La Barbera, C.M. Montone, S. Piovesana, R. Zenezini Chiozzi, A. Laganà, Chromatographic column evaluation for the untargeted profiling of glucosinolates in cauliflower by means of ultra-high performance liquid chromatography coupled to high resolution mass spectrometry, Talanta 179 (2018) 792–802, https://doi.org/10.1016/J.TALANTA.2017.12.019.

[40] L. Song, J.J. Morrison, N.P. Botting, P.J. Thornalley, Analysis of glucosinolates, isothiocyanates, and amine degradation products in vegetable extracts and blood plasma by LC–MS/MS, Anal. Biochem. 347 (2005) 234–243, https://doi.org/10.1016/J.AB.2005.09.040.

[41] C.H. Botting, N.E. Davidson, D.W. Griffiths, R.N. Bennett, N.P. Botting, Analysis of intact glucosinolates by MALDI-TOF mass spectrometry, J. Agric. Food Chem. 50 (2002) 983–988, https://doi.org/10.1021/JF011129A.

[42] Y. Xu, J. Li, Y. Shi, L. Yang, Z. Wang, H. Han, R. Wang, Stereoselective pharmacokinetic study of epiprogoitrin and progoitrin in rats with UHPLC–MS/MS method, J. Pharm. Biomed. Anal. 187 (2020) 113356, https://doi.org/10.1016/J.JPBA.2020.113356.

[43] M.A. Berhow, U. Polat, J.A. Glinski, M. Glensk, S.F. Vaughn, T. Isbell, I. Ayala-Diaz, L. Marek, C. Gardner, Optimized analysis and quantification of glucosinolates from *Camelina sativa* seeds by reverse-phase liquid chromatography, Ind. Crops. Prod. 43 (2013) 119–125, https://doi.org/10.1016/J.INDCROP.2012.07.018.

[44] A.B. Attygalle, S. García-Rubio, J. Ta, J. Meinwald, Collisionally-induced dissociation mass spectra of organic sulfate anions, J. Chem. Soc. Perkin Trans. 2 (2001) 498–506, https://doi.org/10.1039/B009019K.

[45] X. Liang, H.W. Lee, Z. Li, Y. Lu, L. Zou, C.N. Ong, Simultaneous quantification of 22 glucosinolates in 12 Brassicaceae vegetables by hydrophilic interaction chromatography-tandem mass spectrometry, ACS. Omega 3 (2018) 15546–15553, https://doi.org/10.1021/ACSOMEGA.8B01668.

[46] M.T. Engström, M. Pälijärvi, J.-P. Salminen, Rapid fingerprint analysis of plant extracts for ellagitannins, gallic acid, and quinic acid derivatives and quercetin-, kaempferol- and myricetin-based flavonol glycosides by UPLC-QqQ-MS/MS, J. Agric. Food Chem. 63 (2015) 4068–4079, https://doi.org/10.1021/ACS.JAFC.5B00595.

[47] M.T. Engström, M. Pälijärvi, C. Fryganas, J.H. Grabber, I. Mueller-Harvey, J. P. Salminen, Rapid qualitative and quantitative analyses of proanthocyanidin oligomers and polymers by UPLC-MS/MS, J. Agric. Food Chem. 62 (2014) 3390–3399, https://doi.org/10.1021/JF500745Y.

[48] J.E. Laitila, J. Suvanto, J.P. Salminen, Liquid chromatography–tandem mass spectrometry reveals detailed chromatographic fingerprints of anthocyanins and anthocyanin adducts in red wine, Food Chem. 294 (2019) 138–151, https://doi.org/10.1016/J.FOODCHEM.2019.02.136.

[49] V. Fock, A. Agrawal, J.-P. Salminen, Development and application of targeted UHPLC-MS/MS methods for the analysis of 31 groups of cardenolide glycosides, Talanta 298 (2026) 128867, https://doi.org/10.1016/J.TALANTA.2025.128867.

[50] N. Rauniyar, Parallel reaction monitoring: a targeted experiment performed using high resolution and high mass accuracy mass spectrometry, Int. J. Mol. Sci. 16 (2015) 28566–28581, https://doi.org/10.3390/IJMS161226120.

[51] S. Intanon, R.L. Reed, J.F. Stevens, A.G. Hulting, C.A. Mallory-Smith, Identification and phytotoxicity of a new glucosinolate breakdown product from meadowfoam

(*Limnanthes alba*) seed meal, J. Agric. Food Chem. 62 (2014) 7423–7429, https://doi.org/10.1021/JF5018687.
[52] H. Wu, J. Guo, S. Chen, X. Liu, Y. Zhou, X. Zhang, X. Xu, Recent developments in qualitative and quantitative analysis of phytochemical constituents and their metabolites using liquid chromatography–mass spectrometry, J. Pharm. Biomed. Anal. 72 (2013) 267–291, https://doi.org/10.1016/J.JPBA.2012.09.004.
[53] C. Cavaliere, M. Antonelli, A.L. Capriotti, G. La Barbera, C.M. Montone, S. Piovesana, A. Laganà, A triple quadrupole and a hybrid quadrupole orbitrap mass spectrometer in comparison for polyphenol quantitation, J. Agric. Food Chem. 67 (2019) 4885–4896, https://doi.org/10.1021/ACS.JAFC.8B07163.
[54] European Medicines Agency (EMA), ICH Q2(R1) validation of analytical procedures: text and methodology - step 5, in: https://www.ema.europa.eu/en/ich-q2r2-validation-analytical-procedures, 1995 (accessed October 22, 2022).
[55] H. Evard, A. Kruve, I. Leito, Tutorial on estimating the limit of detection using LC-MS analysis, part I: theoretical review, Anal. Chim. Acta 942 (2016) 23–39, https://doi.org/10.1016/J.ACA.2016.08.043.
[56] H. Evard, A. Kruve, I. Leito, Tutorial on estimating the limit of detection using LC-MS analysis, part II: practical aspects, Anal. Chim. Acta 942 (2016) 40–49, https://doi.org/10.1016/J.ACA.2016.08.042.
[57] B.K. Matuszewski, M.L. Constanzer, C.M. Chavez-Eng, Matrix effect in quantitative LC/MS/MS analyses of biological fluids: a method for determination of finasteride in Human plasma at picogram per milliliter concentrations, Anal. Chem. 70 (1998) 882–889, https://doi.org/10.1021/ac971078. +.
[58] R. Mithen, R. Bennett, J. Marquez, Glucosinolate biochemical diversity and innovation in the Brassicales, Phytochemistry 71 (2010) 2074–2086, https://doi.org/10.1016/J.PHYTOCHEM.2010.09.017.
[59] S. Vanhakylä, Distribution of Foliar Plant Polyphenols Across the Plant Phylogeny, University of Turku, 2025. https://urn.fi/URN:ISBN:978-952-02-0228-6.
[60] M. Caban, N. Migowska, P. Stepnowski, M. Kwiatkowski, J. Kumirska, Matrix effects and recovery calculations in analyses of pharmaceuticals based on the determination of β-blockers and β-agonists in environmental samples, J. Chromatogr. A 1258 (2012) 117–127, https://doi.org/10.1016/J.CHROMA.2012.08.029.
[61] J.C. Van De Steene, W.E. Lambert, Comparison of matrix effects in HPLC-MS/MS and UPLC-MS/MS analysis of nine basic pharmaceuticals in surface waters, J. Am. Soc. Mass Spectrom. 19 (2008) 713–718, https://doi.org/10.1016/J.JASMS.2008.01.013.
[62] A. Kruve, I. Leito, K. Herodes, Combating matrix effects in LC/ESI/MS: the extrapolative dilution approach, Anal. Chim. Acta 651 (2009) 75–80, https://doi.org/10.1016/J.ACA.2009.07.060.
[63] J. Moilanen, J. Sinkkonen, J.P. Salminen, Characterization of bioactive plant ellagitannins by chromatographic, spectroscopic and mass spectrometric methods, Chemoecology 23 (2013) 165–179, https://doi.org/10.1007/S00049-013-0132-3.
[64] L.W. Sumner, A. Amberg, D. Barrett, M.H. Beale, R. Beger, C.A. Daykin, T.W. M. Fan, O. Fiehn, R. Goodacre, J.L. Griffin, T. Hankemeier, N. Hardy, J. Harnly, R. Higashi, J. Kopka, A.N. Lane, J.C. Lindon, P. Marriott, A.W. Nicholls, M.D. Reily, J.J. Thaden, M.R. Viant, Proposed minimum reporting standards for chemical analysis Chemical analysis Working Group (CAWG) Metabolomics Standards Initiative (MSI), Metabolomics 3 (2007) 211–221, https://doi.org/10.1007/S11306-007-0082-2.